

Wireless Channel Modeling Perspectives for Ultra-Reliable Communications

Patrick C. F. Eggers and Petar Popovski

Antennas, Propagation and Radio Networking (APNET)

Department of Electronic Systems, Aalborg University, Denmark

Abstract

Ultra-Reliable Communication (URC) is one of the distinctive features of the upcoming 5G wireless communication. The level of reliability, going down to packet error rates (PER) of 10^{-9} , should be sufficiently convincing in order to remove cables in an industrial setting or provide remote control of robots with mission-critical function. In this paper we present elements of physical and statistical modeling of the wireless channel that are relevant for characterization of the lower tail of the channel Cumulative Distribution Function (CDF). There are channel models, such as Two-Wave with Diffuse Power (TWDP) or Suzuki, where finding the full CDF is not tractable. We show that, for a wide range of channel models, the outage probability at URC levels can be approximated by a simple expression, whose exponent depends on the actual channel model. Furthermore, it is seen that the two-wave model leads to pessimistic predictions of the fading in the region of ultra-reliable communications, while the CDFs of models that contain diffuse components have slopes that correspond to the slope of a Rayleigh fading. We provide analysis of the receive antenna diversity schemes for URC-relevant statistics and obtain a new expression for Maximum Ratio Combining (MRC) in Weibull channels.

Index Terms

Ultra-reliable communications, 5G, wireless channel models, fading, diversity, probability tail approximations.

I. INTRODUCTION

One of the features of 5G wireless communication systems is to offer wireless communication with extremely high reliability guarantees, also known as *Ultra-Reliable Communication (URC)* [1]. The level of reliability, going sometimes down to packet error rates (PER) of 10^{-8} , should be sufficiently convincing in order to remove cables in an industrial setting, remote control of

robots and drones that need to perform a critical function, remote surgery or self-driving cars [2]. A significant number of the URC use cases take place indoors, which resonates with the expectation for a wireless environment that is, to some extent, controlled and offers predictable signal quality. Wireless communication performance is inherently a stochastic variable; however, URC refocuses our attention to the statistical characterization of the rare events and the lower tail of the channel Cumulative Distribution Function (CDF). This requires a major effort in terms of measurement campaigns, purposefully designed to capture the lower tail statistics, as well as in terms of analytical channel modeling.

Nevertheless, a good starting point for characterizing wireless channels is to analyze the current channel models in regimes that are relevant for URC, which is the topic of this article. The related works [3], [4] have characterized the probability density functions of wireless channel models, often leading to very complex expression and analysis dependent on multiple parameters. Our objective is to get insight into the behavior of different channel models at the region of *ultra-low error rates*, which we define as a PER that is $\epsilon \leq 10^{-5}$ or lower, corresponding to the reliability of “five nines”. Different mission-critical services will use different levels of ultra-reliability, such as PERs of 10^{-6} in smart grids and 10^{-9} for factory automation [2]. We focus on the packet errors that occur due to outages, induced by block fading, rather than noise-induced errors. Recent studies [5] have shown that this is a very suitable model for transmission of short packets, which are in turn expected to be prevalent in the URC scenarios. Throughout the paper we will use the term *URC-relevant statistics* to denote the events in signal reception that occur with probabilities on the order of 10^{-5} or less. Our analysis shows that, despite the complex probability density functions, the behavior of the lower tail can be significantly simplified, leading to important insights on the behaviors that occur when the outage probabilities are very low. Furthermore, it is confirmed that the two-wave model with equal amplitudes of the two waves represents one of the most pessimistic cases in terms of URC-relevant statistics.

Besides the analysis of various statistical channel models, in this paper we also revisit the basic assumptions adopted in channel modeling in the light of the statistically rare events that needs to be captured in an URC regime. The existing channel models have been developed for wireless communication systems¹ that deal with bit error rates (BER) of 10^{-3} to 10^{-4} [6] and

¹First generation digital system like GSM, with emphasis on voice communication. Frame(voice) or block(data) error rates (decoded) are one or two order of magnitudes above the nominal raw BER.

there is a lack of experimental evidence to support channel models that deal with PER of 10^{-6} or 10^{-8} . This paper extrapolates the standard channel models towards URC-relevant statistics and identifies their limitations when modeling rare events. Our main result is that, for a wide range of channel models, the tail approximation of the cumulative distribution function at the URC levels has the form:

$$F\left(\frac{P_R}{A}\right) \approx \alpha \left(\frac{P_R}{A}\right)^\beta \quad (1)$$

where A is the average power, P_R is the minimal required power to decode the packet correctly and α, β are parameters that depend on the actual channel model. Specifically, the exponent β determines how the error probability depends on the minimal required power. While the tuning of the models can only be done with appropriate experimental evidence, this work provides a valuable contribution to the modeling efforts that are essential for designing ultra-reliable wireless systems.

The paper is organized as follows. After the introduction, in Section II we introduce the system model. Section III contains physical/statistical considerations for two canonical deployment models. Section IV contains analysis of the URC-relevant tail probability for various channel models. Section V contains the analysis of the receive diversity schemes in URC regime. Section VI concludes the paper.

II. SYSTEM MODEL AND BASIC MODELING ASSUMPTIONS

The model used in this paper is related to the complex baseband model of a narrowband channel with reduced wave grouping from [3]:

$$V = \sum_{i=1}^N \rho_i e^{j\phi_i} + V_{\text{dif}} \quad (2)$$

where V is the received complex voltage, ρ_i/ϕ_i is the amplitude/phase of the i -th specular component and V_{dif} is the diffuse component. The physical basis for the model in [3] is created by a single scattering process. Hence, the component V_{dif} is treated in its simplest form, as a contribution from a large number of waves and application of the central limit theorem, which leads to:

$$V_{\text{dif}} = X_R + jX_I \quad (3)$$

where X_R and X_I are independent Gaussian variables, each with zero mean and variance σ^2 . This type of diffuse component and absence ($N = 0$) of specular components leads to the

classical Rayleigh channel. Regarding the specular components, in [3] it is assumed that each ρ_i is constant and that ϕ_i is a uniform random variable.

The model used in our analysis generalizes the model from [3] in multiple ways. For the specular components, we will relate ρ_i and ϕ_i to the physical setup and discuss the validity of the assumption on a random uniform ϕ_i . Furthermore, ρ_i will not be necessarily treated as constant and it can be subject to, e.g. log-normal shadowing. A more general variant of the diffuse component can be derived when multi-scatter physical setup is considered [7]. This will lead to the cases of Weibull and Cascaded Rayleigh channel, as well as compound channels, such as Suzuki. Throughout the paper we will treat the models of narrowband channel.

An underlying assumption is the one of block fading, such that the power at which the packet is received remains constant and equal to $P = |V|^2 = r^2$, where V is given by (2) and $r = |V|$ is the envelope. We assume that the noise power is normalized to 1, such that P also denotes the Signal-to-Noise Ratio (SNR) at which a given packet is received. For each new packet, all random variables from (2) are independently sampled from their probability distributions². The average received power for the channel model (2) across many realizations is denoted by

$$A = E[P] = \sum_{i=1}^N E[|V_i|^2] + E[|V_{\text{dif}}|^2] \stackrel{(a)}{=} \sum_{i=1}^N \rho_i^2 + 2\sigma^2 \quad (4)$$

where $E[\cdot]$ denotes the expectation operator and (a) is valid when we treat the reduced wave grouping model from [3]. Let R denote the transmission rate of the packet. We assume that packet errors occur due to outage only, such that the PER ϵ is given by:

$$\epsilon = \Pr(R < \log_2(1 + P)) = \Pr(P < P_R) \quad (5)$$

where $P_R = 2^R - 1$ is the minimal required power to receive the packet sent at rate R .

In propagation modeling it is common to build a wireless channel model by assuming separability of the following effects [8]:

- Path loss, dependent on the actual geometric setting and operating frequency.
- Long-term fading effects, which is typically shadowing as a means to model macroscopic effects that change over a long period of time.
- Short-term fading effects, relevant for a time scale of a packet (quasi-static fading) or even a symbol (fast fading), assuming stationary scattering conditions.

²The reader may object that this assumption is not valid when long-term shadowing is treated, i.e. a sample for a given ρ_i is applicable to several packet transmissions. See Section IV-H for discussion about this assumption.

The performance of URC, and especially of URC with low latency, called URLLC in the 5G terminology [2], is affected by the short-term statistics and its (un)predictability in order to determine the fate of packet reception. Assuming separability of effects, the statistics of short-term fading is based on parameters that are derived from the other two effects (long-term fading and path loss) and those parameters are assumed constant over a short term. However, separability becomes problematic when we consider channel models for URC-level statistics. The reason is that the estimation of the long-term parameters requires certain level of accuracy in order for the short-term statistics to be a valid indicator for an event that occurs less than e.g. 10^{-5} fraction of the time.

A final remark is in order. When considering rare events in the region of URC-relevant statistics, one has to take into account the precision of the equipment, as well as the reliability of the equipment and the environment, such as, e.g., the installation and the physical surroundings. It is impossible to take all those effects into account in a single paper, but we believe that the discussion presented here can initiate similar reliability-based analysis that pertains to those factors.

III. PHYSICS OF PROPAGATION IN CANONICAL DEPLOYMENT MODELS

In order to provide insights about the impact that the physical parameters have on the signal statistics relevant for URC, we consider two canonical deployment models, outdoor and indoor, respectively. The models are simplified, but sufficient to bring forward the main physical phenomena that have an impact on channel statistics.

A. Outdoor Deployment Model

We start with the simple two-path propagation model [8] in order to set a physical ground for revising the assumption of uniform random phase. The received signal has only two specular components:

$$V = \rho_1 e^{j\phi_1} + \rho_2 e^{j\phi_2} = \frac{G\lambda}{4\pi d_L} e^{-j\frac{2\pi}{\lambda}d_L} + \Gamma \frac{G\lambda}{4\pi d_R} e^{-j\frac{2\pi}{\lambda}d_R}$$

where G is a parameter dependent on the antenna gains, λ is the wavelength, d_L/d_R is the distance of the Line-of-sight(LoS)/reflected path and Γ is the reflection coefficient. The key role for the received signal strength is played by $\Delta d = d_R - d_L$, which in turn can be determined

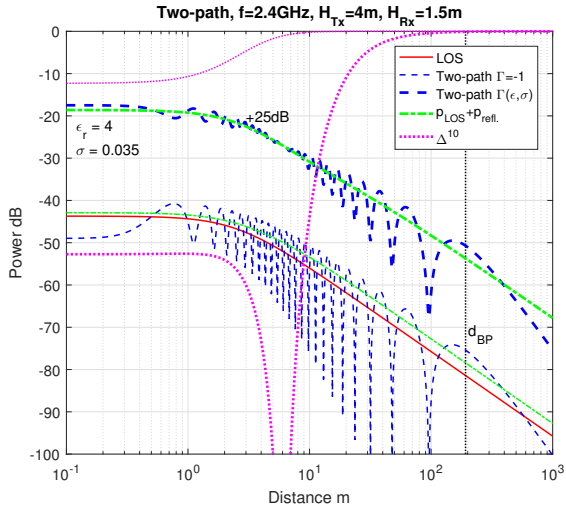


Fig. 1. Two-path model behavior for two different surface materials.

by the distance between the transmitter TX and the receiver RX, as well as the corresponding antenna heights H_{TX} and H_{RX} .

Fig. 1 depicts the received power in a two-path model using using pico-cell like geometries with $H_{\text{TX}} = 4\text{m}$ and $H_{\text{RX}} = 1.5\text{m}$. The assumed operating frequency is 2.4GHz. Two different reflection coefficients are used. The case $\Gamma = -1$ is a sensible approximation valid for far distances, with very low impinging angle of reflected signal. The other case $\Gamma(\epsilon_r)$ represents surface materials, such as soil or concrete, with relative dielectric constant $\epsilon_r = 4$ and conductivity of 0.035 S/m, found in urban settings and use of angular-dependent reflection coefficient for vertical polarization (eq. (3.1.19) in [8]). For clarity, the curves are plotted with an offset of 25 dB. For each reflection coefficient, we plot both the actual power of the signal, based on the vector sum and the sum of the power of both components. Finally, we also plot the peak to average ratio of specular powers

$$\Delta = \frac{2\rho_1\rho_2}{\rho_1^2 + \rho_2^2} \quad (6)$$

defined in [3], here zoomed by a factor 10 on the dB scale. As d increases beyond a certain distance, different phase rotations start to provoke alternating constructive and destructive interference ripples, i.e. fading. It is easily shown that by increasing d beyond a breakpoint $d_B = \frac{4\pi H_{\text{TX}} H_{\text{RX}}}{\lambda}$, the phases converge to full cancellation, i.e. a phase difference of π . At distances beyond d_B no fading occurs. We can represent the received signal with a model that has two

specular components and the following envelope:

$$r = |\rho_1 + \rho_2 e^{j\phi_2}| \quad (7)$$

where we have assumed that $\phi_1 = 0$ without affecting the resulting envelope and the received power is $P = r^2$. Fig. 1 suggests that there are three different zones of signal behavior: (1) LoS-dominated region as long as $\Delta \lesssim -1$ dB, seen as a single vector whose power decays as d^2 ³. (2) A “ripple” zone up to distance d_B . (3) Cancellation region for distances beyond d_B , seen as a single vector whose power decays as d^4 .

The received power according to the distance is a *deterministic* function and in order to obtain a certain channel statistics, we need to induce a random process. One way to do it would be to select randomly the distance between the TX and the RX; however, in that case we randomize ρ_1, ρ_2 and ϕ_2 . Another randomization can be obtained by fixing the distance to keep a constant average power $A = \rho_1^2 + \rho_2^2$ and assume that ϕ_2 is changed by a small *perturbation*, such as e.g. perturbation in the TX/RX heights or in the frequency. The small perturbations do not affect d_L and d_R , and thereby ρ_1 and ρ_2 , significantly. It is seen that in zones 1 and 3 the small perturbation results in small changes in the received power, which means that the two-wave model with uniform distribution of ϕ_2 is not applicable. However, in the zone 2 small perturbations result in large changes of the received power, since ϕ_2 is affected significantly. This can be approximated by a two-wave model (7) with constant ρ_1, ρ_2 and uniform random ϕ_2 . Given ρ_1 and ρ_2 , the minimal envelope that can be obtained for $\phi_2 = \pi$ is $r_{\min} = |\rho_1 - \rho_2|$.

In a picocell geometry, the ripple region, and therefore the two-wave model, has a significant role. Its size is determined by the antenna heights as well as the reflective property of the surface material, which in turn determines Δ . The ripple region ranges from few meters for a highly reflective ground up to tens of meters for common building materials, where $\Delta > -1$ dB. When $\Delta = 0$ dB, we have $\rho_1 = \rho_2$ and full cancellation can occur with $r_{\min} = 0$. In this case, the two-wave model represents a severe fading scenario, exhibiting dynamics that is worse than the Rayleigh fading, as also shown analytically in Section IV. For example, for PER of 10^{-6} and $\Delta = 0$, the ratio $\frac{P_R}{A}$ is of order -120 dB, which prohibits the practical planning of URC. However, this is a strongly singular case that provides an upper bound on the tail of the error probability.

³the d^2 decay does not appear in first part in Fig. 1, as d is only the horizontal path component. For $d < H_{\text{TX}}$, the total path distance (and thus power) appears near constant.

The discussion above refers only to the behavior of the specular components. In a realistic deployment scenario, a diffuse component will appear due to multiple scatterers and rough surfaces. This will, intuitively, mask the vector balancing and help avoid the severe fading cases in a two-wave model that occur when $\Delta = 1$. In this case, the tail of the error probability will depend on the power ratio of the specular components and the diffuse component, called *k-factor*:

$$k_N = \frac{\sum_{i=1}^N \rho_i^2}{2\sigma^2} \quad (8)$$

We have seen that ρ_i depends on the distance, but the diffuse power can also depend on it. For simplicity, in outdoor scenarios we can reasonably model the diffuse power to be proportional to the dominant component power so the *k*-factor appears constant with distance [9]. This can be argued by treating the effective scattering area as constant in size with respect to the distance (e.g. dominated by urban structures) and it is illuminated with power density that corresponds to the dominant components. In a more complex model, the *k*-factor would vary according to the shadowing of the specular components.

B. Indoor Deployment Model

Consider a typical small boiler room with dimensions length \times width \times height of $10 \times 8 \times 3$ m³, antenna heights $H_{\text{TX}} = H_{\text{RX}} = 1.5$ m and operating frequency of 2.4 GHz. Differently from the outdoor case with a single reflecting surface, here the bounded volume can provoke dominant specular reflections from all surfaces, provided they have sufficiently large sections of smooth surface (windows, doors etc.). Fig. 2 illustrates the received power by placing the TX at the center of one of the side walls and moving the RX within the room. In the calculation we consider $N = 6$ specular components: four in the vertical radial plane (LoS, floor reflection, ceiling reflection and a reflection from the wall behind the RX) and two in the horizontal transverse plane due to the side walls. We use same material properties as in the outdoor example for the floor, while we simplify the reflective properties of the other walls, assuming reduction by factors 0.5 (back/side walls) and 0.33 (ceiling) of the specular reflection compared to the ideally smooth surface. Finally, we assume that only the first order reflections result in specular components, while all further reflections are absorbed into a diffuse term.

Referring to Fig. 2, the dominance of the LoS component causes a smooth decrease of the average power as the RX moves towards the back wall. The stronger ripple pattern at a distance

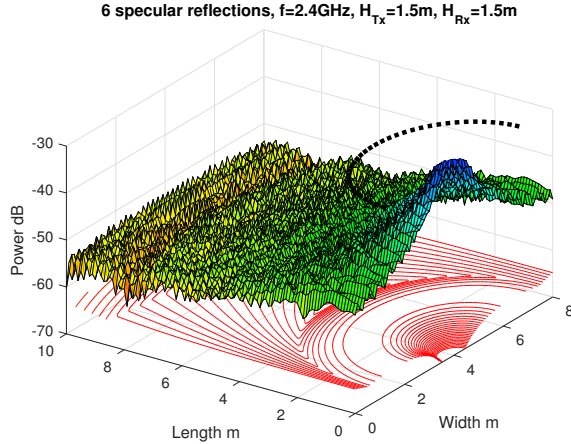


Fig. 2. Received power in an indoor scenario assuming six dominant components. One sample is taken per one $10 \times 10 \text{ cm}^2$ square. For a frequency of 2.4 Ghz, the wavelength is $\lambda = 8 \text{ cm}$. Here $H_{\text{TX}} = H_{\text{RX}} = 1.5 \text{ m}$.

1 – 3 m from the TX is due to the effect of a strong second specular component that comes from floor reflection. Each contour at the bottom denotes a set of spatial points for which the value of Δ , calculated for the two strongest components, is constant. For practical values of the material in the room it is always $\Delta < 1$. The dashed circle of radius 2.8 m at a level of -30 dB depicts the *reverberation distance* [10] where the power of the LoS and the diffuse components are equal. In the room electromagnetic theory [10], the equilibrium between the power launched (P_{TX}) and absorbed in the room is used to determine the diffuse power P_{dif} through the ratio:

$$\frac{P_{\text{dif}}}{P_{\text{TX}}} = \frac{\lambda^2}{4\pi^2\eta A} \quad (9)$$

where A is the total room absorption due to all surfaces and $\eta = 0.5$ is the average absorption coefficient, introduced in order to adjust the diffuse power level to the experimental findings [10]. Here the diffuse power level is independent from the location, such that the k -factor decreases as the specular components decrease, which is a significant difference from the outdoor case. In summary, diffuse power has a significant impact in the case of indoor deployment, leaning the model towards statistics that is dominated by the diffuse component.

IV. LOWER TAIL STATISTICS FOR COMMON CHANNEL MODELS

In this section we present the analytical models and approximations for the behavior of some commonly used channel models in the region of the lower tail, which represents URC-relevant

TABLE I

CDF TAIL APPROXIMATIONS F , FOR DISTRIBUTIONS IN THE FOLLOWING SUBSECTIONS. VALIDITY POWER LIMITS ($p = P_R/A$) AND LOG-LOG SLOPE $\beta = \frac{d \log(F)}{d \log(p)}$. BRACKETED ENTRIES $(\cdot)^*$, INDICATE SPECIAL SOLUTIONS.

Distribution	Tail $\sim F(p) _{p \rightarrow 0}$	Limits	Slope $\sim \beta$
Two Wave (TW)	$\frac{1}{2} - \frac{1}{\pi} \arcsin\left(\frac{1-p}{\Delta}\right)$	$1 - \Delta \leq p \leq 1 + \Delta$	$(\frac{1}{2})^*$
Three Wave (3W)	$\frac{P_R}{4\pi\Delta_r}$	$\frac{r_{\min}^2}{A} \leq p < \rho_1^2(\Delta_\rho ^2)^*/A$	$1 (\frac{1}{2}, \frac{3}{4})^*$
Rayleigh (Rayl)	p	$0 \leq p < 1$	1
Rice	$F_{\text{Rayl}}(p(k_1 + 1)) e^{-k_1}$	$0 \leq p < \frac{1}{4k_1(k_1 + 1)}$	1
TW with Diffuse Power (TWDP)	$F_{\text{Rice}}(p; k_2) I_0(k_2\Delta)$	$0 \leq p < \frac{1}{4k_2(k_2 + 1)}$	1
Weibull (Wei)	$(\Gamma(1 + 1/\beta)p)^\beta$	$0 \leq p < 1/\Gamma(1 + 1/\beta)$	β
Cascaded Rayleigh (Cas)	$-p \frac{1+\Gamma}{1-\Gamma} \ln\left(p \frac{1+\Gamma}{(1-\Gamma)^2}\right)$	$0 \leq p < \frac{1}{4} \frac{(1-\Gamma)^2}{1+\Gamma}$	$1 + \frac{1}{\ln(p) + \ln \frac{1+\Gamma}{(1-\Gamma)^2}}$
Log-Normal (LN)	$\frac{1}{4} e^{-\frac{(\frac{1}{2} \ln(P_R) - a\sigma_l - \mu_l)^2}{2\sigma_l^2}}$	$0 \leq p < e^{-2\sigma_l^2}$	$\frac{10}{\ln 10} \left[\frac{a}{\sigma_{\text{dB}}} - 2 \frac{P_{R,\text{dB}} - \mu_{\text{dB}}}{2\sigma_{\text{dB}}^2} \right]$
Suzuki (Suz)	$P_R 10^{\frac{1}{10}(\sigma_{\text{dB}}^2(\frac{\ln 10}{20}) - \mu_{\text{dB}})}$	$0 \leq p < e^{-8\sigma_l^2}$	1

statistics. Given the target packet error probability (PER) or outage probability of ϵ , for each model the objective is to find P_R , defined in (5) through the following CDF $F(P_R)$:

$$\epsilon = F(P_R) = \int_{r_{\min}}^{\sqrt{P_R}} f(x) dx \quad (10)$$

where x is the received envelope and r_{\min} is the minimal value of the envelope in the support set of $f(x)$, which is the Probability Density Function (PDF). The approximations in the following text will be made under the assumption that ϵ is very small.

Table I collects all tail approximations from this paper in one place. The detailed derivation for each of the distributions is given in the sequel.

A. Two-Wave Model

In this model $N = 2$, $V_{\text{dif}} = 0$ and the received envelope is given by (7). The average received power is $A_{\text{TW}} = \rho_1^2 + \rho_2^2$ and the PDF of the envelope is given by:

$$f_{\text{TW}}(r) = \frac{2r}{\pi A_{\text{TW}} \sqrt{\Delta^2 - \left(1 - \frac{r^2}{A_{\text{TW}}}\right)^2}}$$

where Δ is given by (6) and $r \in [r_{\min}, r_{\max}] = [\sqrt{A_{\text{TW}}(1 - \Delta)}, \sqrt{A_{\text{TW}}(1 + \Delta)}]$. By putting $f_{\text{TW}}(r)$ in (10) we get:

$$\epsilon = F_{\text{TW}}(P_R) = \frac{1}{2} - \frac{1}{\pi} \arcsin\left(\frac{1 - \frac{P_R}{A_{\text{TW}}}}{\Delta}\right) \quad (11)$$

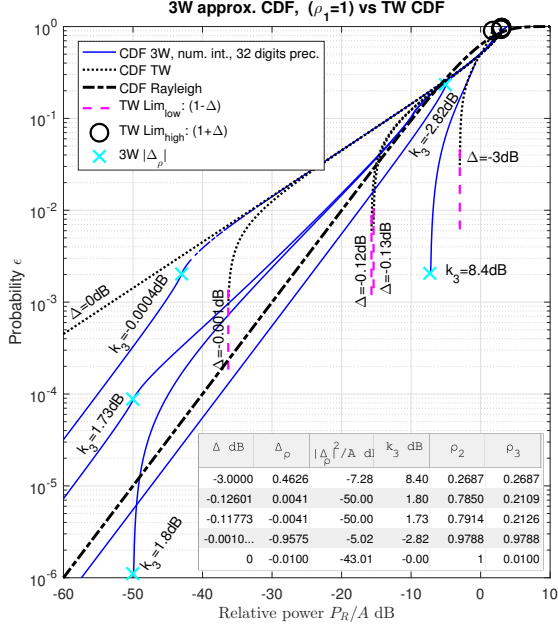


Fig. 3. Two-wave and three-wave distributions for various parameters.

which results in

$$P_R = F_{\text{TW}}^{-1}(\epsilon) = A_{\text{TW}}(1 - \Delta \cos(\pi\epsilon)) \approx A_{\text{TW}} \left(1 - \Delta + \Delta \frac{(\pi\epsilon)^2}{2}\right) \quad (12)$$

In the special case $\Delta = 1$ we get:

$$P_R = F_{\text{TW}}^{-1}(\epsilon) \approx A_{\text{TW}} \frac{(\pi\epsilon)^2}{2} \quad (13)$$

When $\Delta < 1$, the minimal value of the received power is $(1 - \Delta) > 0$. Note that $\Delta = 1$ is a rather singular case in which the received envelope can go to $r_{\min} = 0$. The case $\Delta \approx 1$ has been referred to in the literature as hyper-Rayleigh fading [11]. Furthermore, the logarithmic relation for $\Delta = 1$ is:

$$\log \epsilon = \text{const.} + \frac{1}{2} \log P_R \quad (14)$$

i.e. with a log-log linear slope of $\beta \approx \frac{1}{2}$.

Fig. 3 shows the CDF of $\frac{P_R}{A_{\text{TW}}}$. The CDF obtains zero value when $P_R = r_{\min}^2$, such that when $\Delta < 1$, the CDF goes abruptly to zero at $\frac{r_{\min}^2}{A_{\text{TW}}}$. However, as it is seen from Fig. 3, the log-log slope that precedes this abrupt transition to zero is $\frac{1}{2}$, i.e. half a decade per 10 dB. This slope continues until $-\infty$ (in dB) in the singular case $\Delta = 1 = 0$ dB. For example, if the log-log

slope of $\frac{1}{2}$ should be present at $\epsilon = 10^{-6}$, then we need to have $\Delta > -4 \cdot 10^{-6}$ dB, i.e. ρ_2 very close to ρ_1 . This justifies the term “singular” for $\Delta = 0$ dB, since even small deviation of Δ from 0 dB changes the pessimistic choice of R and P_R . Hence, the two-wave model should be used with caution when evaluating URC scenarios.

B. Three-Wave Model

In this model $N = 3$, $V_{\text{dif}} = 0$, the received envelope is:

$$r = |\rho_1 + \rho_2 e^{j\phi_2} + \rho_3 e^{j\phi_3}| \quad (15)$$

and average power $A_{3W} = \sum_{n=1}^3 \rho_n^2$. The probability density function [3], [12] is given by:

$$f_{3W}(r) = \begin{cases} \frac{\sqrt{r}}{\pi^2 \sqrt{\rho_1 \rho_2 \rho_3}} K\left(\frac{\Delta_r^2}{\rho_1 \rho_2 \rho_3 r}\right) & \Delta_r^2 \leq \rho_1 \rho_2 \rho_3 r \\ \frac{r}{\pi^2 \Delta_r} K\left(\frac{\rho_1 \rho_2 \rho_3 r}{\Delta_r^2}\right) & \Delta_r^2 > \rho_1 \rho_2 \rho_3 r \end{cases} \quad (16)$$

for $r \in [r_{\min}, r_{\max}]$, and it is 0 otherwise, where:

$$\begin{aligned} r_{\min} &= \max(2 \max(\rho_1, \rho_2, \rho_3) - \rho_1 - \rho_2 - \rho_3, 0) \\ r_{\max} &= \rho_1 + \rho_2 + \rho_3 \end{aligned} \quad (17)$$

In (16), $K(\cdot)$ is an elliptic integral of the first kind⁴ and the quantity Δ_r is defined as:

$$\Delta_r^2 = \frac{1}{16} [(r + \rho_1)^2 - (\rho_2 - \rho_3)^2][(r - \rho_1)^2 - (\rho_2 + \rho_3)^2] \quad (18)$$

Without losing generality, we can take $\rho_1 \geq \rho_2 \geq \rho_3$ and define the difference $\Delta_\rho = \rho_1 - (\rho_2 + \rho_3)$, such that $r_{\min} = \max(\Delta_\rho, 0)$. Three cases can be considered: (1) $r_{\min} = 0$ when $\Delta_\rho < 0$; (2) $r_{\min} = 0$ and $\Delta_\rho = 0$; and (3) $r_{\min} > 0$ otherwise. Here we treat the case $\Delta_\rho < 0$, which sets the basis for the reader to treat the other two cases. The integral (10) is evaluated for values $r \in [0, \sqrt{P_R}]$ that are very small and taking $r \rightarrow 0$:

$$\lim_{r \rightarrow 0} \Delta_r^2 = [\rho_1^2 - (\rho_2 - \rho_3)^2][(\rho_2 + \rho_3)^2 - \rho_1^2] > 0 \quad (19)$$

which implies that $\Delta_r^2 > \rho_1 \rho_2 \rho_3 r$ holds in (16). With $r \rightarrow 0$:

$$f_{3W}(r) \xrightarrow{r \rightarrow 0} \frac{r}{\pi^2 \Delta_r} K\left(\frac{\rho_1 \rho_2 \rho_3 r}{\Delta_r^2}\right) \approx \frac{r}{\pi^2 \Delta_r} \frac{\pi}{2} \quad (20)$$

⁴Convention of [12], [3] is $K(m)$ with argument $m = k^2$ (instead of $K(k)$ with modulus k).

where we have used $\lim_{x \rightarrow 0} K(x) = \frac{\pi}{2}$. Approximating Δ_r^2 as a constant for small values of r , we get:

$$\epsilon = F_{3W}(P_R) \approx \frac{r^2}{4\pi\Delta_r} = \frac{P_R}{4\pi\Delta_r} \quad (21)$$

such that the log-log linear slope is $\beta \approx 1$. In the singular case $r_{\min} = 0$ and $\Delta_\rho = 0$ it can be shown that $\beta = \frac{3}{4}$, while the case $r_{\min} > 0$ has a slope of $\frac{1}{2}, \frac{3}{4}$ or 1, before an abrupt fall to zero when $P_R = r_{\min}^2$.

The 3W CDF, generated with high-precision numerical integration, is shown on Fig. 3 for $\rho_1 = 1$ and different variations of ρ_2 and ρ_3 . Each curve of the 3W model is labeled by $k_3 = \frac{\rho_1^2}{(\rho_2^2 + \rho_3^2)}$ and the table on the lower right corner shows the parameters for the different 3W cases. There are two cases with identical $10 \log \frac{|\Delta_\rho|^2}{P} = -50$ dB that are seen to diverge significantly when $\frac{P_R}{A_{3W}} < -40$ dB. The difference between these two cases emerges due to the different sign of Δ_ρ , which in one case results in $r_{\min} > 0$ and in the other case $r_{\min} = 0$. The latter case has a log-log slope of $\beta = 1$, identical to the Rayleigh distribution (see the next section). Hence, if the sum of the two other specular components is sufficiently strong to cancel and overshoot the strongest component, the URC-level behavior of the 3W model is practically identical to that of a Rayleigh channel in terms of a slope, with a certain offset from the actual Rayleigh curve. In other words, three specular components that lead to $\Delta_\rho < 0$ are sufficient to produce the behavior of a Rayleigh diffuse component.

C. Rayleigh Channel

This model, adopted in many wireless studies, has $N = 0$ and only a diffuse component V_{dif} that consists of Gaussian variables. The received envelope is:

$$r = |X_R + jX_I| \quad (22)$$

with the classical probability density function [13]:

$$f_{\text{Rayl}}(r) = \frac{2r}{A_{\text{Rayl}}} e^{-\frac{r^2}{A_{\text{Rayl}}}} \quad (23)$$

and average power $A_{\text{Rayl}} = 2\sigma^2$. The cumulative solution follows readily as

$$\epsilon = F_{\text{Rayl}}(P_R) = 1 - e^{-\frac{P_R}{A_{\text{Rayl}}}} \quad (24)$$

which for $\epsilon \rightarrow 0$ is approximated by

$$P_R = F_{\text{Rayl}}^{-1}(\epsilon) = -A_{\text{Rayl}} \ln(1 - \epsilon) \approx A_{\text{Rayl}}\epsilon, \quad (25)$$

$$\log \epsilon \approx \log \frac{P_R}{A_{\text{Rayl}}} \quad (26)$$

leading to the Rayleigh rule of thumb “10dB outage margin per decade probability” due to a log-log slope of $\beta \approx 1$.

D. Rician Channel

This model features a specular component mixed with the diffuse one, such that the received envelope is $r = |\rho_1 + V_{\text{dif}}|$. The average received power is $A_{\text{Rice}} = \rho_1^2 + 2\sigma^2 = 2\sigma^2(k_1 + 1)$, where $k_1 = \frac{\rho_1^2}{2\sigma^2}$ is the Rician k -factor and the probability density function is [13]:

$$f_{\text{Rice}}(r) = f_{\text{Rayl}}(r) e^{-k_1} I_0 \left(\frac{r}{\sigma} \sqrt{2k_1} \right) \quad (27)$$

where $I_0(\cdot)$ is the modified Bessel function of 1st kind and 0th order. The CDF lower tail can be extracted from [14] polynomial expansion of the Marcum Q function, while here we derive lower and upper bounds on the CDF.

To get the lower bound, we observe that $I_0(x) \geq 1$ and $\lim_{x \rightarrow 0} I_0(x) = 1$. This corresponds to $\frac{P_R}{P_{\text{Rice}}} \ll \frac{1}{4k_1(k_1+1)}$ and the tail of the CDF translates to a scaled Rayleigh as:

$$\epsilon = F_{\text{Rice}}(P_R) \geq F_{\text{Rayl}}(r) e^{-k_1} = \left(1 - e^{-\frac{P_R}{A_{\text{Rice}}}(k_1+1)} \right) e^{-k_1} \quad (28)$$

which leads to the approximation:

$$\log \epsilon \approx \log \frac{P_R}{A_{\text{Rice}}} + \log(k_1 + 1) - \frac{k_1}{\ln(10)} \quad (29)$$

i.e. with Rayleigh slope $\beta \approx 1$, where the tightness of the bound and the offset from the Rayleigh slope depend on k_1 .

An upper bound can be derived by using the result from [15] that $I_0(x) < e^{x^2/4}$. With this we can approximate $f_{\text{Rice}}(r) \approx \frac{r}{\sigma^2} e^{-\frac{r^2}{2\sigma^2}(1-k_1)} e^{-k_1}$ and the CDF tail is:

$$\epsilon = F_{\text{Rice}}(P_R) < \left(1 - e^{-\frac{P_R}{A_{\text{Rice}}}(1-k_1^2)} \right) \frac{e^{-k_1}}{1 - k_1} \quad (30)$$

For small values of $\frac{P_R}{A_{\text{Rice}}}$, the asymptotic log-log slope of ϵ with respect to P_R is $\beta \approx 1$. It is however, important to note from Fig. 4 that before attaining the slope $\beta = 1$, the Rician CDF has a steeper slope compared to the Rayleigh one. In the context of wireless communications, this can be interpreted as an increased diversity order offered by the Ricean distribution. However, the lower the k_1 -factor, the sooner the slope of the Ricean CDF becomes identical to the Rayleigh one. The change of the slope in Fig. 4 is indicated by circles.

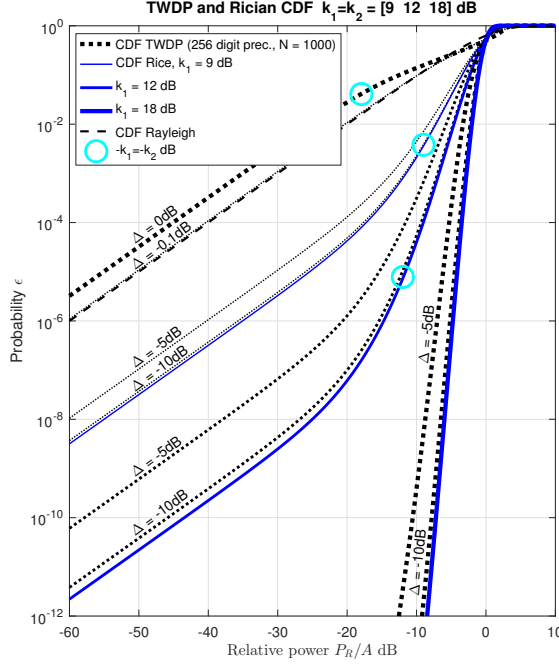


Fig. 4. Rician and TWDP distributions for different values of the relevant parameters.

Using same approximation as in (29), we can invert (28) as

$$P_R = F_{\text{Rice}}^{-1}(\epsilon) \approx \epsilon A_{\text{Rice}} \frac{e^{k_1}}{k_1 + 1} \quad (31)$$

E. Two-Wave Diffuse Power (TWDP) Channel

In this model $N = 2$ and V_{dif} , with envelope $r = |\rho_1 + \rho_2 + V_{\text{dif}}|$ and average received power $A_{\text{TWDP}} = \rho_1^2 + \rho_2^2 + 2\sigma^2$ [3]. The PDF is obtained by averaging of the Rician PDF [4]:

$$f_{\text{TWDP}}(r) = \frac{1}{2\pi} \int_0^{2\pi} f_{\text{Rice}}(r; k_2 [1 + \Delta \cos(\psi)]) d\psi \quad (32)$$

with Δ defined in (6) and k_2 in (8). The integration over ψ involves only $I_0(\cdot)$ and the exponential terms in (27). Using again $I_0 \approx 1$ for $\frac{P_R}{A_{\text{TWDP}}} \ll \frac{1}{4k_2(k_2+1)}$, this integration is $\sim \frac{1}{2\pi} \int_0^{2\pi} e^{k_2 \Delta \cos \psi} \cdot 1 d\psi = I_0(k_2 \Delta)$, i.e. it leads to a constant with respect to r , such that the resulting CDF is a scaled Rician CDF:

$$\epsilon = F_{\text{TWDP}}(P_R) \approx F_{\text{Rice}}(P_R; k_2) I_0(k_2 \Delta) \quad (33)$$

$$P_R = F_{\text{TWDP}}^{-1}(\epsilon) \approx F_{\text{Rice}}^{-1}\left(\frac{\epsilon}{I_0(k_2 \Delta)}; k_2\right) \quad (34)$$

and thus the analysis from the previous Rician case can be directly applied, scaled by $I_0(k_2\Delta)$. From Fig. 4 it can be seen that TWDP⁵ starts to differ from a Rician model (with $k_1 = k_2$) when Δ is sufficiently high, such that ρ_2 can be distinguished from V_{dif} . The second specular component ρ_2 lifts-off the lower tail as $\Delta \rightarrow 0\text{dB}$, while preserving the Rayleigh tail slope. For $k_2 \approx 10\text{dB}$ and having $\Delta = -0.1\text{dB}$, the Rician CDF matches closely the Rayleigh CDF. Note that, in order to reach the extreme slope of the singular TW model at the URC levels, one needs $\Delta = 0\text{dB}$ and k_2 in range 50 to 60dB; this is very unlikely to happen in practice.

F. Weibull Channel

This model consists of a diffuse component only, but the distribution of it follows the Weibull model. This is a generalization of the Rayleigh model, where the diffuse component is given by $V_{\text{dif}} = (X_R + jX_I)^{1/\beta}$ and it can be $\beta \neq 1$. The Weibull model has been used in empirical studies as it offers increased freedom to fit the modeling of the diffuse part [17], [18], [19]. The received envelope $r = |V_{\text{dif}}|$ has a PDF given by [20]:

$$f_{\text{Wei}}(r) = \frac{2\beta r^{2\beta-1}}{2\sigma^2} e^{-\frac{r^{2\beta}}{2\sigma^2}} \quad (35)$$

with shape parameter $k = 2\beta > 0$ and scale parameter $\lambda = (2\sigma^2)^{1/2\beta} > 0$, $A_{\text{Wei}} = (2\sigma^2)^{1/\beta} \Gamma(1 + 1/\beta)$. For $\beta = \frac{1}{2}$ we have the extreme TW case, while $\beta = 1$ leads to the Rayleigh case. The CDF is given as:

$$\epsilon = F_{\text{Wei}}(P_R) = 1 - e^{-\left(\Gamma(1+1/\beta)\frac{P_R}{A_{\text{Wei}}}\right)^\beta} \quad (36)$$

which leads to:

$$P_R = F_{\text{Wei}}^{-1}(\epsilon) = \frac{A_{\text{Wei}}}{\Gamma(1 + 1/\beta)} (-\ln(1 - \epsilon))^{1/\beta} \approx \frac{A_{\text{Wei}}}{\Gamma(1 + 1/\beta)} \epsilon^{1/\beta}$$

$$\log \epsilon \approx \beta \left(\log \frac{P_R}{A_{\text{Wei}}} + \log \Gamma(1 + 1/\beta) \right) \quad (37)$$

where we have used the same type of approximation as in the Rayleigh case. Here β denotes the log-log slope.

⁵No tractable closed form of PDF or CDF exists. In [3] the PDF is approximated, while we use a complete expansion by [16]. However, due to the numerical sensitivity at URC levels, it requires the use of high-precision numerical tools.

G. Cascaded Rayleigh Channel

This model also contains only a diffuse component, which is a product of the envelopes of two Rayleigh links r_1 and r_2 . The compound received envelope is $r = r_1 r_2 = |X_{R_1} + jX_{I_1}| \cdot |X_{R_2} + jX_{I_2}|$ with PDF equal to [21], [22]⁶:

$$f_{\text{Cas}}(r) = \frac{r_\Gamma}{\sigma_1 \sigma_2} I_0 \left(r_\Gamma \sqrt{\Gamma} \right) K_0(r_\Gamma) \quad (38)$$

where $r_\Gamma = \frac{r}{\sigma_1 \sigma_2 (1-\Gamma)}$. Using (38) we get $A_{\text{Cas}} = E[r^2] = 4\sigma_1^2 \sigma_2^2 (1+\Gamma) = \bar{P}_1 \bar{P}_2 (1+\Gamma)$ with correlation coefficient Γ between powers $P_1 = r_1^2$ and $P_2 = r_2^2$. I_n and K_n are the Modified Bessel functions of 1st and 2nd kind, of order n . The CDF follows as:

$$\epsilon = F_{\text{Cas}}(P_R) = 1 - r_\Gamma [\sqrt{\Gamma} \cdot I_1 \left(r_\Gamma \sqrt{\Gamma} \right) K_0(r_\Gamma) + I_0 \left(r_\Gamma \sqrt{\Gamma} \right) K_1(r_\Gamma)] \quad (39)$$

Approximating the Bessel functions for $r_\Gamma \ll 1$, the general case ($\Gamma < 1$) simplifies as

$$\begin{aligned} \epsilon = F_{\text{Cas}}(P_R) &\approx -\frac{r_\Gamma^2}{4} (1-\Gamma) \left[2 \ln \left(\frac{r_\Gamma}{2} \right) + (2\gamma - 1) \right] \\ &\approx -\frac{P_R}{A_{\text{Cas}}} \frac{1+\Gamma}{1-\Gamma} \ln \left(\frac{P_R}{A_{\text{Cas}}} \frac{1+\Gamma}{(1-\Gamma)^2} \right) \end{aligned} \quad (40)$$

where $\gamma = 0.5772..$ is Eulers constant. The log probability is:

$$\log(\epsilon) \approx \log \frac{P_R}{A_{\text{Cas}}} + \log \frac{1+\Gamma}{1-\Gamma} + \log \left(-\ln \left(\frac{P_R}{A_{\text{Cas}}} \frac{1+\Gamma}{(1-\Gamma)^2} \right) \right) \quad (41)$$

and is valid below the knee point $\frac{P_R}{A_{\text{Cas}}} \ll \frac{1}{4} \frac{(1-\Gamma)^2}{1+\Gamma}$. The slope is found as the the first derivative of $\log(\epsilon)$ w.r.t. $\log \frac{P_R}{A_{\text{Cas}}}$, leading to $\beta \approx 1 + \frac{1}{\ln \left(\frac{P_R}{A_{\text{Cas}}} \right) + \ln \frac{1+\Gamma}{(1-\Gamma)^2}}$ and it gradually approaches a Rayleigh slope for $\frac{P_R}{A_{\text{Cas}}} \rightarrow 0$. For $\Gamma = 0$ the model collapses to the well known double-Rayleigh model [25].

When $\epsilon < 1/e$, the function in (40) can be inverted [26] via a single Lambert W branch [27]:

$$P_R = F_{\text{Cas}}^{-1}(\epsilon) \approx -A_{\text{Cas}} \epsilon \frac{1-\Gamma}{1+\Gamma} \frac{1}{W_{-1} \left(-\frac{\epsilon}{1-\Gamma} \right)} \quad (42)$$

For the singular case of $\Gamma = 1 (r_1 = r_2)$, simple deduction yields $r_{\text{Cas}} = r_1 r_2 = F_{\text{Cas}}^{-1}(\epsilon) = F_{\text{Rayl}}^{-1}(\epsilon)^2 = r_{\text{Rayl}}^2$. Thus, $F_{\text{Cas}}(P_R) = F_{\text{Rayl}}(\sqrt{P_R}) \sim \sqrt{\frac{P_R}{A_{\text{Rayl}}}}$ and the slope $\beta \approx \frac{1}{2}$ is identical to the singular case of a TW model. It can be concluded from Fig. 5 that a the log-log behavior of cascaded Rayleigh fading can be represented by two different slopes with a breakpoint.

⁶Ref. [22] uses the convention $\Gamma = \Gamma_{V_1, V_2}$, whereas we use $\Gamma = \Gamma_{P_1, P_2}$ as in [21]. Note that for Rayleigh fading $|\Gamma_{V_1, V_2}|^2 = \Gamma_{X_{R_1}, X_{R_2}}^2 + \Gamma_{X_{R_1}, X_{I_2}}^2 = \Gamma_{P_1, P_2} \approx \Gamma_{r_1, r_2}$ and $\Gamma_{X_{R_1}, X_{I_2}}^2 \approx 0$ for random links [23], [24].

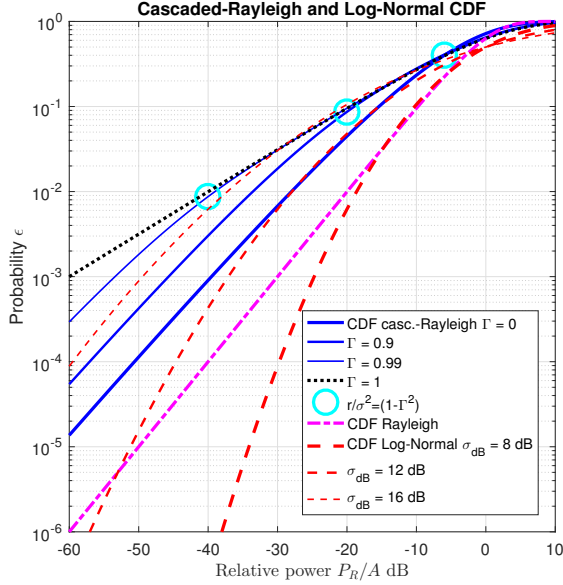


Fig. 5. Cascaded Rayleigh and Log-Normal distributions for different values of the parameters.

H. Log-Normal Channel

In this model there is a single specular component $N = 1$ and no diffuse component. The specular component is not constant, but subject to a log-normal shadowing, such that log-envelope $\ln(r)$ is modeled as Gaussian variable [13], [8] with PDF:

$$f_{\text{LN}}(r) = \frac{1}{r} \mathcal{N}_{\ln(r)}(\mu_l, \sigma_l) = \frac{1}{r \sigma_l \sqrt{2\pi}} e^{-\frac{(\ln(r) - \mu_l)^2}{2\sigma_l^2}} \quad (43)$$

with logarithmic mean and standard deviation $\mu_l = E[\ln(r)] = \mu_{\text{dB}} \frac{\ln(10)}{20}$ and $\sigma_l = \sqrt{E[\ln(r)^2] - \mu_l^2} = \sigma_{\text{dB}} \frac{\ln(10)}{20}$. The average power is $A_{\text{LN}} = e^{2\sigma_l^2 + 2\mu_l}$ [8] and the CDF

$$\epsilon = F_{\text{LN}}(r) = \frac{1}{2} + \frac{1}{2} \text{erf}\left(\frac{\ln(r) - \mu_l}{\sigma_l \sqrt{2}}\right) \quad (44)$$

with $x = (\ln(r) - \mu_l)/(\sigma_l \sqrt{2})$ and erf being the error function. Using Bürmann-type asymptotic approximation [28] leads to $F_{\text{LN}}(x) \approx \frac{1}{2} \left(1 + \text{sgn}(x) \sqrt{1 - e^{-x^2}}\right) \approx \frac{1}{4} e^{-x^2}$, when omitting higher order terms and approximating the square root for $|x| \gg 0$. A tighter approximation can be obtained if we use $F_{\text{LN}}(x) \approx \frac{1}{4} e^{-f(x)}$ with a polynomial fitting function $f(x)$ [29][30]. Comparing $\frac{1}{4} e^{-x^2}$ with (44), it appears to be shifted proportionally to σ_l , such that:

$$\epsilon = F_{\text{LN}}(P_R) \approx \frac{1}{4} e^{-\frac{\left(\frac{1}{2} \ln(P_R) - \alpha \sigma_l - \mu_l\right)^2}{2\sigma_l^2}} \quad (45)$$

$$\log \epsilon \approx \log \frac{1}{4} - \frac{1}{\ln(10)} \frac{(P_{R,\text{dB}} - a\sigma_{\text{dB}} - \mu_{\text{dB}})^2}{2\sigma_{\text{dB}}^2} \quad (46)$$

With $a = 0.223$, the relative error $|\epsilon_{\text{rel}}(P_R)| = \left| \frac{\epsilon_{\text{approx}}(P_R)}{\epsilon_{\text{LN}}(P_R)} - 1 \right| \lesssim 10^{-1}$ for $10^{-12} \leq \epsilon \leq 10^{-2}$ and $3 \leq \sigma_{\text{dB}} \leq 24 \text{ dB}$. The deviation on the margin matters most for outage analysis and is here below $\frac{1}{3} \text{ dB}$. This accuracy is still very useful, considering the simplicity of the expression for analytical studies.

Finding a root of the second order equation in $\ln(P_R)$ (45) we get

$$P_R = F_{\text{LN}}^{-1}(\epsilon) \approx e^{2[(a\sigma_l + \mu_l) + \sqrt{2\sigma_l \sqrt{-\ln(\epsilon) + \ln(1/4)}}]} \quad (47)$$

For a given P_R , we can find the log-log slope as $\beta = \frac{d \log(F_{\text{LN}})}{d \log(P_R)} \approx \frac{10}{\ln 10} \left[\frac{a}{\sigma_{\text{dB}}} - 2 \frac{P_{R,\text{dB}} - \mu_{\text{dB}}}{2\sigma_{\text{dB}}^2} \right]$. Clearly, the log-log relationship is not linear as we have seen in the other models. From Fig. 5 it is observed that, for large σ_{dB} , a log-normal channel can exhibit extreme slopes when the level $\frac{P_R}{A}$ is in the region -20 to -40 dB, which makes it hard to distinguish from a TW or TWDP channel. However, when going towards URC-relevant levels, the deviation from a linear slope is noticeable.

The log-normal model is distinctive from the previous models in at least two aspects. *First*, the probability of outage is calculated based on a block fading model, where the sender selects the transmission rate R and the channel through which this transmission is carried out is independently sampled from a given distribution. However, if we consider transmission of multiple packets within a short time span, the instance of log-normal shadowing is highly likely to be correlated, which gives the sender the opportunity to adapt the data rate R and avoid outage or at least decrease the probability of it. Hence, with respect to the channel dynamics, this analysis of a log-normal channel should be understood as a pessimistic one. It is applicable to a scenario where the sender transmits sporadically and between two transmissions the environment changes significantly, leading to new independent log-normal sample. *Second*, as indicated above, the slope is not linear, but in practical measurements this could be mistaken for a statistical effect of insufficient number of samples.

I. Suzuki Channel

This is a compound channel consist of a diffuse component only, which is a mixture between a Rayleigh envelope and Log-Normal varying mean [31], [8]. The compound envelope is $r = |X_R + jX_I|$, where X_R and X_I are zero-mean Gaussian variables with variance $\sigma_{\text{LN}} = e^{\mathcal{N}}$ that has

a log-normal distribution. Following the discussion in the previous section, one can think of the Suzuki channel model to be applicable to the following situation. When there is only Rayleigh block fading, the outage probability can be controlled by selecting the rate R according to the known average power of the Rayleigh channel. However, when the sender does not have a reliable estimate of the average power, then this uncertainty can be modeled by assuming that the average power is log-normal distributed. This is an illustration of the non-separability of effects, indicated in Section II. Again, as in the previous section, the independent sampling from the log-normal distribution is a pessimistic case that assumes sporadic transmissions, sufficiently separated in time.

The PDF and CDF of the Suzuki channel can be found as follows. Let us denote by A the average power used to generate Rayleigh-faded power level A . The power A is log-normal distributed, such that we can obtain its PDF from the PDF of the log-normal envelope (43) by substituting $A = r^2$. This leads to the following joint distribution of P and A :

$$f_{\text{Suz}}(P, A) = \frac{1}{A} e^{-\frac{P}{A}} \cdot \frac{1}{2A\sigma_l\sqrt{2\pi}} e^{-\frac{(\frac{1}{2}\ln A - \mu_l)^2}{2\sigma_l^2}} \quad (48)$$

For given P_R , the outage probability can be calculated as follows:

$$\epsilon = \int_0^{P_R} dP \int_0^{\infty} f_{\text{Suz}}(P, A) dA \quad (49)$$

The distribution $f_{\text{Suz}}(P, A)$ can be rewritten as follows:

$$f_{\text{Suz}}(P, A) = \frac{1}{2A^2\sigma_l\sqrt{2\pi}} e^{-\frac{(\frac{1}{2}\ln A - \mu_l)^2}{2\sigma_l^2} - \frac{P}{A}} \quad (50)$$

The upper bound for (49) is obtained by noting that $\frac{P}{A} \geq 0$ and it can be removed from (50), after which we get:

$$\begin{aligned} \epsilon &\leq \int_0^{P_R} dP \int_0^{\infty} \frac{1}{2A^2\sigma_l\sqrt{2\pi}} e^{-\frac{(\frac{1}{2}\ln A - \mu_l)^2}{2\sigma_l^2}} dA \\ &= e^{2\sigma_l^2 - 2\mu_l} P_R = \frac{P_R}{A_{\text{Suz}}} \cdot 2e^{4\sigma_l^2} \end{aligned} \quad (51)$$

where $A_{\text{Suz}} = 2e^{2\sigma_l^2 + 2\mu_l} = 2A_{\text{LN}}$ [32].

The lower bound can be found by using the inequality $e^{-x} \geq 1 - x$ which leads to:

$$f_{\text{Suz}}(P, A) \geq \frac{1}{2A^2\sigma_l\sqrt{2\pi}} e^{-\frac{(\frac{1}{2}\ln A - \mu_l)^2}{2\sigma_l^2}} (1 - \frac{P}{A}) \quad (52)$$

and results in

$$\epsilon \geq \frac{P_R}{A_{\text{Suz}}} 2e^{4\sigma_l^2} - \left(\frac{P_R}{A_{\text{Suz}}} \right)^2 \cdot 2e^{12\sigma_l^2} \quad (53)$$

For URC-relevant levels it is $P_R \ll A_{\text{Suz}}$, such that the upper bound can be treated as tight and the log-log relation is:

$$\log \epsilon \approx \log \frac{P_R}{A_{\text{Suz}}} + \log 2 + 4\sigma_{\text{dB}}^2 \frac{\ln(10)}{20^2} \quad (54)$$

leading to the Rayleigh-like slope of $\beta = 1$. Under the same assumptions, inversion of (51) yields

$$P_R = F_{\text{Suz}}^{-1}(\epsilon) \approx \frac{1}{2}\epsilon A_{\text{Suz}} e^{-4\sigma_l^2} \quad (55)$$

V. SIMPLIFIED ANALYSIS OF DIVERSITY SCHEMES

So far we have determined the URC-relevant statistics of various channel models by assuming a single antenna at the receiver. In practice, attaining very high reliability levels with reasonable power can only happen by having high levels of diversity at the receiver. Our analysis has shown that the tail approximation at the URC levels mostly has the form given in (1), which can be used for simplified diversity analysis, in particular in cases in which the full PDF/CDF are not tractable. In the previous sections our analysis has focused chiefly on β , while the scaling α need to be extracted from the tail expressions explicitly. The factor α can be composed of two factors: (1) the tail offset of the distribution α_{CDF} determined by the distribution of the channel model; (2) α_{ant} due to branch power ratio (BPR), defined for a pair of the m -th and n -th antenna as $\text{BPR}_{nm} = \frac{A_n}{A_m}$. Hence, $\alpha = \alpha_{\text{CDF}}\alpha_{\text{ant}}$.

For small terminals, the main impairment towards exploiting multi-antenna (multi-branch) diversity is the BPR [33], [34], [35]. On the other hand, when operating in higher frequency bands, the terminal dimensions become comparable or larger than the wavelength, which leads to low branch correlations. Hence, in the following we assume that the receiver has M antennas that are not correlated.

In selection combining (SC), only the strongest signal among the M antennas is selected:

$$P_{R,\text{SC}} = \max(P_1, \dots, P_M) \quad (56)$$

For independent branches, we get:

$$\epsilon = F_{\text{SC}}(P_R) = \prod_{m=1}^M F_m(P_R) \quad (57)$$

When Maximum Ratio Combining (MRC) is used, the received power is:

$$P_{R,\text{MRC}} = \sum_{m=1}^M P_m \quad (58)$$

When considering the Rayleigh case, a general solution for the CDF with MRC is involved. For uncorrelated Rayleigh branch signals, tractable solutions exist when all BPR= 1 or all BPR \neq 1 [8], [13], [36]. However, [36] has a simple approximation for the MRC PDF for low powers, valid for all BPRs, which can be used to obtain:

$$\epsilon = F_{\text{MRC}}(P_R) \sim \underbrace{\frac{1}{M!}}_{\alpha_{\text{MRC}}} \prod_{m=1}^M \alpha_m P_R = \underbrace{\frac{1}{M!}}_{\alpha_{\text{MRC}}} P_R^M \prod_{m=1}^M \alpha_m \quad (59)$$

which has simple product form as in SC, shifted by $\alpha_{\text{MRC}} = \frac{1}{M!}$. This expression is valid for all channel models where $\beta \approx 1$ and the coefficients α_m are branch normalizations depending on the mean power as well as the tail offset for the specific channel model (Rice, TWDP, etc.).

In Appendix A we have derived a simple Weibull MRC tail approximation, valid for all slope and BPR branch combinations. As this solution also appears in a weighted form of the SC solution, it is easy to make a heuristic generic expansion by considering local log-log linear approximation of the CDF tails. This is the case for Log-Normal and Cascaded Rayleigh models, where the branch slopes depend on the power levels $\beta(P_R/A)$, such that:

$$\epsilon = F_{\text{MRC}}(P_R) \approx \alpha_{\text{MRC}}(\beta_1(P_R)..\beta_M(P_R)) \cdot F_{\text{SC}}(P_R) \quad (60)$$

with α_{MRC} given in (62) or simplified in (63) when all branches have the same log-log slope.

Fig. 6 shows Monte Carlo simulation with 10^8 samples of TWDP, Log-Normal and Double-Rayleigh (Cascaded Rayleigh with $\Gamma = 0$) distributions with different mean powers. Each distribution is further circularly shifted to provide uncorrelated copies for i.i.d. $M = 4$. It is observed how the single branch tail approximations (thin lines) follow the simulations up to the onset of the shoulders. For the TWDP approximation, it is $-k_2$ dB from the mean level. The 4-branch MRC tail approximation shows very good fit at URC probabilities - bold dots indicate point of 1dB deviation to the simulation. Furthermore, it is observed from the Log-Normal and 3-branch cross-distribution MRC, that the heuristic expansion in (60) indeed provides very useful results.

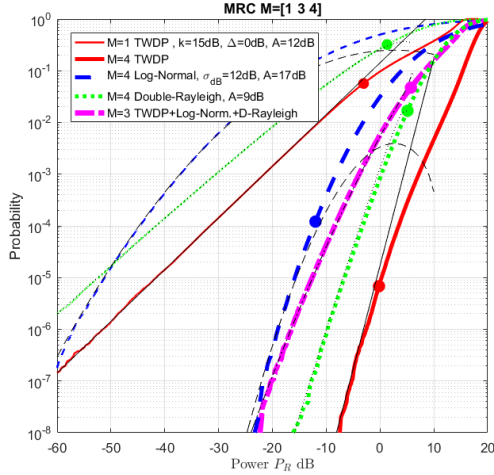


Fig. 6. MRC with $M = 4$ for i.i.d. TWDP, Log-Normal and Double-Rayleigh (Cascaded Rayleigh with $\Gamma = 0$) with uncorrelated signals. Also MRC with $M = 3$ for one branch of each of the distributions. Bolder curves are obtained by simulation, thin lines are the tail approximations. (33), (40), (45) and MRC (60), (62)

VI. DISCUSSION AND CONCLUSIONS

In this paper we have investigated the properties of wireless channel models in the URC regime and developed approximations of the tail distributions. We have provided insights in the connection between the physical and statistical properties by considering canonical deployment scenarios. Furthermore, our analysis has shown that, for a wide range of practical models, the outage probability at URC levels depends on the minimal required decoding power through an exponent β which, for the case of Rayleigh fading is $\beta \approx 1$. Interestingly, the same exponent is asymptotically valid a wide selection of physically few-path and multi-path models. We have seen that hyper-Rayleigh fading, confirmed empirically for wireless communications with modest reliability requirements (outage rate 10^{-3} at -30 dB), can result in an exponent $\beta = \frac{1}{2}$ at URC

levels, which leads to very conservative, if at all useful, rate selection. Distributions that can lead to hyper-Rayleigh fading, such as two-wave, three-wave, or Two Wave with Diffuse Power (TWDP), are the ones where the dominant paths can be cancelled. Thus, when conducting empirical studies that work with these models, one should account for the large uncertainty that occurs when assessing the models at the URC levels and collect proportionally large number of samples. Finally, we have provided a simplified analysis of several diversity schemes, which paves the way for more elaborate analysis of various diversity schemes, which are, on the other hand, vital for achieving URC operation with reasonable data rates.

ACKNOWLEDGMENT

This work was supported by the H2020 European Research Council (Consolidator Grant Nr. 648382 WILLOW).

APPENDIX A MRC FOR WEIBUL RANDOM VARIABLES

Here we treat the case of MRC for independent non-identically distributed (i.n.i.d.) Weibull random variables. MRC PDF solution for independent random variables (RV), is obtainable via convolution of the branch PDFs $f_1 * f_2 * \dots * f_m$, e.g. through the multiplication of moment generating functions (MGF) $\prod M_m$ and inverse Laplace transform \mathcal{L}^{-1} . However, following such approach for approximating the full CDF of Weibull MRC involves Meijer-G or Fox-H functions [37], [20], [38], which are too complex to readily extract a simple tail approximation. This difficulty persists for other simplifications of MGF or MRC PDF [39], [40], [41]. On the other hand, note that, to get the tail approximation for MRC with independent branch powers, it is sufficient to deal with branch tail PDFs only [42]. The lower tail of the Weibull PDF (35) can be approximated as:

$$f_{\text{Wei}}(P_R) = f_{\text{Wei}}(r = \sqrt{P_R}) \left| \frac{dr}{dP_R} \right|_{P_R \rightarrow 0} \approx \frac{\beta}{2\sigma^2} P_R^{\beta-1} \quad (61)$$

Using Laplace transform relation [43, ET I 137(1), Table 17.13] $F(s) = \mathcal{L}(f(t)) = 1/s^\nu \leftrightarrow f(t) = t^{\nu-1}/\Gamma(\nu)$, the branch $F_{\text{Wei}}(s) \approx \frac{\beta}{2\sigma^2} \frac{\Gamma(\beta)}{s^\beta}$. The Weibull i.n.i.d M-branch MRC CDF (for any BPR or β combination), is established as $F_{\text{Wei},\text{MRC}}(P_R) = \mathcal{L}^{-1} \left(\frac{1}{s} \prod_{m=1}^M F_{\text{Wei},m}(s) \right)$, where

$\frac{1}{s}$ is used to produce the CDF from the inverse transform. Using the same Laplace relation as before, we arrive at

$$\begin{aligned} F_{\text{Wei,MRC}}(P_R) &\approx \mathcal{L}^{-1} \left(\frac{1}{s \prod_{m=1}^M s^{\beta_m}} \right) \cdot \prod_{m=1}^M \frac{\beta_m \Gamma(\beta_m)}{2\sigma_m^2} \\ &= \underbrace{\frac{\prod_{m=1}^M \Gamma(1 + \beta_m)}{\Gamma(1 + \sum_{m=1}^M \beta_m)} \prod_{m=1}^M \Gamma(1 + \frac{1}{\beta_m})^{\beta_m}}_{\alpha_{\text{MRC}}} \underbrace{\frac{P_R^{\sum_{m=1}^M \beta_m}}{\prod_{m=1}^M A_m^{\beta_m}}}_{\sim F_{\text{SC}} = \prod F_{\text{Wei},m}} \quad (62) \end{aligned}$$

with Weibull mean relation $2\sigma^2 = (\frac{A}{\Gamma(1+1/\beta)})^\beta$. It should be noted that the solution splits into a MRC weighting term α_{MRC} (which correctly collapses to 1 for $M = 1$) and a SC-like solution term ($F_{\text{SC}} = \prod F_m$). When all branch slopes are equal $\beta_m = \beta$, we get:

$$F_{\text{Wei,MRC}}(P_R) \approx \underbrace{\frac{\Gamma(1 + \beta)^M}{\Gamma(1 + \beta M)} \frac{\Gamma(1 + \frac{1}{\beta})^{\beta M}}{\prod_{m=1}^M \text{BPR}_m^\beta}}_{\alpha_{\text{MRC}}} \underbrace{\left(\frac{P_R}{A_1}\right)^{\beta M}}_{\sim F_{\text{SC}} = \prod F_{\text{Wei},m}} \quad (63)$$

with $\text{BPR}_m = A_m/A_1$. A heuristic simplification is $\alpha_{\text{MRC}} \sim \frac{1}{M!^\beta}$, with deviation $\lesssim 1\text{dB}$ for $M = 4$ and 1.5dB for $M = 8$ at 10^{-6} probability, for $\frac{1}{2} \lesssim \beta \lesssim 2$. For the particular Rayleigh case of $\beta = 1$, the solution collapses to the known result of (59).

REFERENCES

- [1] P. Popovski, “Ultra-reliable communication in 5G wireless systems,” in *Proceedings of the 1st International Conference on 5G for Ubiquitous Connectivity (5GU)*, Levi, Finland, 2014, pp. 146–151.
- [2] P. Schulz, M. Matthe, H. Klessig, M. Simsek, G. Fettweis, J. Ansari, S. A. Ashraf, B. Almeroth, J. Voigt, I. Riedel *et al.*, “Latency critical IoT applications in 5G: Perspective on the design of radio interface and network architecture,” *IEEE Communications Magazine*, vol. 55, no. 2, pp. 70–78, 2017.
- [3] G. D. Durgin, T. S. Rappaport, and D. A. De Wolf, “New analytical models and probability density functions for fading in wireless communications,” *IEEE Transactions on Communications*, vol. 50, no. 6, pp. 1005–1015, 2002.
- [4] M. Rao, F. J. Lopez-Martinez, M.-S. Alouini, and A. Goldsmith, “MGF approach to the analysis of generalized two-ray fading models,” *IEEE Transactions on Wireless Communications*, vol. 14, no. 5, pp. 2548–2561, 2015.
- [5] G. Durisi, T. Koch, and P. Popovski, “Toward massive, ultrareliable, and low-latency wireless communication with short packets,” *Proceedings of the IEEE*, vol. 104, no. 9, pp. 1711–1726, 2016.
- [6] *Digital cellular telecommunications system (Phase 2+); Radio transmission and reception*, TS 145 005 V10.8.0, ETSI standard, 2014.
- [7] J. B. Andersen and I. Z. Kovacs, “Power distributions revisited,” in *COST273 3rd Management Committee Meeting*, 2002, pp. 17–18.
- [8] R. Vaughan and J. B. Andersen, *Channels, propagation and antennas for mobile communications*. IET, 2003, vol. 50.
- [9] X. Zhao, T. Jämsä, J. Meinilä, P. Kyösti, J.-P. Nuutinen, D. Laselva, and L. Hentilä, “Measurements and modelling of the small scale effects of radio channels for rural and suburban b3g wireless communications,” *14th IST Mobile & Wireless Communications Summit, Dresden, Germany*, 2005.

- [10] J. B. Andersen, J. Nielsen, G. Pedersen, G. Bauch, and J. Herdin, "Room electromagnetics," *IEEE Antennas and Propagation Magazine*, vol. 49, no. 2, pp. 27–33, 2007.
- [11] J. Frolik, "On appropriate models for characterizing hyper-rayleigh fading," *IEEE Transactions on Wireless Communications*, vol. 7, no. 12, 2008.
- [12] J. Nicholson, "Generalisation of a theorem due to Sonine," *Quart. J. Math.*, vol. 48, pp. 321–329, 1920.
- [13] W. C. Jakes, *Microwave mobile communications*. Wiley-IEEE Press, 1994.
- [14] M. Pent, "Orthogonal polynomial approach for the Marcum Q-function numerical computation," *Electronics Letters*, vol. 4, no. 25, pp. 563–564, 1968.
- [15] Á. Baricz, "Bounds for modified Bessel functions of the first and second kinds," *Proceedings of the Edinburgh Mathematical Society (Series 2)*, vol. 53, no. 03, pp. 575–599, 2010.
- [16] S. A. Saberli and N. C. Beaulieu, "New expressions for TWDP fading statistics," *IEEE Wireless Communications Letters*, vol. 2, no. 6, pp. 643–646, 2013.
- [17] R. Lorenz, "Theoretical distribution functions of multipath fading processes in the mobile radio and determination of their parameters by measurements," *Technisher Bericht (in German)*, vol. 455, 1979.
- [18] N. S. Adawi, H. Bertoni, J. Child, W. Daniel, J. Dettra, R. Eckert, E. Flath, and R. Forrest, "Coverage prediction for mobile radio systems operating in the 800/900 MHz frequency range," *IEEE Transactions on Vehicular Technology*, vol. 37, no. 1, p. 3, 1988.
- [19] H. Hashemi, "The indoor radio propagation channel," *Proceedings of the IEEE*, vol. 81, no. 7, pp. 943–968, 1993.
- [20] A. Bessate and F. El Bouanani, "A very tight approximate results of MRC receivers over independent Weibull fading channels," *Physical Communication*, vol. 21, pp. 30–40, 2016.
- [21] M. K. Simon and M.-S. Alouini, *Digital communication over fading channels*. John Wiley & Sons, 2005, vol. 95.
- [22] Y. A. Chau and K. Y.-T. Huang, "On the second-order statistics of correlated cascaded rayleigh fading channels," *International Journal of Antennas and Propagation*, vol. 2012, 2012.
- [23] D. E. Kerr, *Propagation of short radio waves*. IET, 1951, vol. 24.
- [24] J. N. Pierce and S. Stein, "Multiple diversity with nonindependent fading," *Proceedings of the IRE*, vol. 48, no. 1, pp. 89–104, 1960.
- [25] V. Erceg, S. J. Fortune, J. Ling, A. Rustako, and R. A. Valenzuela, "Comparisons of a computer-based propagation prediction tool with experimental data collected in urban microcellular environments," *IEEE Journal on Selected Areas in Communications*, vol. 15, no. 4, pp. 677–684, 1997.
- [26] Maplesoft, *Maple User Manual*, Maplesoft, Waterloo, ON Canada, 2017, version 18. [Online]. Available: <http://www.maplesoft.com>
- [27] R. M. Corless, G. H. Gonnet, D. E. G. Hare, D. J. Jeffrey, and D. E. Knuth, "On the LambertW function," *Advances in Computational Mathematics*, vol. 5, no. 1, pp. 329–359, 1996.
- [28] H. M. Schöpf and P. H. Supancic, "On Bürmann's theorem and its application to problems of linear and nonlinear heat transfer and diffusion," *The Mathematica Journal*, vol. 16, pp. 1–44, 2014.
- [29] H. Hamaker, "Approximating the cumulative normal distribution and its inverse," *Applied Statistics*, vol. 27, no. 1, pp. 76–77, 1978.
- [30] S. Winitzki. (2008) A handy approximation for the error function and its inverse. Assessed: 23-04-2017. [Online]. Available: <https://sites.google.com/site/winitzki sergei-winitzkis-files>
- [31] H. Suzuki, "A statistical model for urban radio propagation," *IEEE Transactions on Communications*, vol. 25, no. 7, pp. 673–680, 1977.

- [32] C. S. Withers and S. Nadarajah, "A Generalized Suzuki Distribution," *IEEE Wireless Personal Communications*, vol. 62, pp. 807–830, 2012.
- [33] V. Plicanic, B. K. Lau, A. Derneryd, and Z. Ying, "Actual diversity performance of a multiband diversity antenna with hand and head effects," *IEEE Transactions on Antennas and Propagation*, vol. 57, no. 5, pp. 1547–1556, 2009.
- [34] B. R. Yanakiev, J. Ødum Nielsen, M. Christensen, and G. Frølund Pedersen, "Correlation measurements on small mobile devices," in *Antennas and Propagation (EUCAP), 2012 6th European Conference on*. IEEE, 2012, pp. 382–385.
- [35] J. Ødum Nielsen, B. Yanakiev, S. Caporal Del Barrio, and G. Frølund Pedersen, "On antenna design objectives and the channel capacity of mimo handsets," *IEEE Transactions on Antennas and Propagation*, vol. 62, no. 6, pp. 3232–3241, 2014.
- [36] M. Schwartz, W. R. Bennett, and S. Stein, *Communication Systems and Techniques*. McGraw-Hill -IEEE Press, 1996.
- [37] N. C. Sagias, G. K. Karagiannidis, D. A. Zogas, P. T. Mathiopoulos, S. A. Kotsopoulos, and G. S. Tombras, "Performance of diversity receivers over non-identical Weibull fading channels," in *2004, IEEE 59th Vehicular Technology Conference. VTC 2004-Spring*, vol. 1. IEEE, 2004, pp. 480–484.
- [38] F. E. Bouanani, "A new closed-form approximations for MRC receiver over non-identical Weibull fading channels," in *2014 International Wireless Communications and Mobile Computing Conference (IWCMC)*. IEEE, 2014, pp. 600–605.
- [39] A. G. Rossberg, "Laplace transforms of probability distributions and their inversions are easy on logarithmic scales," *Journal of Applied Probability*, vol. 45, no. 2, pp. 531–541, 2008.
- [40] S. Nadarajah and S. Kotz, "On the Weibull MGF," *IEEE Transactions on Communications*, vol. 55, no. 7, p. 1287, 2007.
- [41] F. Yilmaz and M.-S. Alouini, "Sum of Weibull variates and performance of diversity systems," in *IWCWC '09 Proceedings of the 2009 International Conference on Wireless Communications and Mobile Computing: Connecting the World Wirelessly*. IEEE, 2009, pp. 247–252.
- [42] P. Hitczenko and S. Montgomery-Smith, "A note on sums of independent random variables," in *Advances in Stochastic Inequalities, Contemporary Mathematics 234*, T. Hill and C. Houdre, Eds. Providence R.I., USA: A.M.S., 1999, pp. 69–73.
- [43] I. Gradshteyn and I. Ryzhik, *Table of Integrals, Series, and Products*, 7th ed. USA: Academic Press/ Elsevier, 2007.